Baroclinic-to-barotropic pathway in El Niño/Southern Oscillation teleconnections from the viewpoint of a barotropic Rossby wave source

Xuan Ji, J. David Neelin*, and C. Roberto Mechoso

Department of Atmospheric and Oceanic Sciences, University of California, Los Angeles, Los Angeles, California

Corresponding author address: J. David Neelin, Department of Atmospheric and Oceanic Sciences, UCLA, 7127 Math Science Building, 405 Hilgard Avenue, Los Angeles, CA 90095-1565.
E-mail: neelin@atmos.ucla.edu

ABSTRACT

The baroclinic-to-barotropic pathway in ENSO teleconnections is examined from the viewpoint of a barotropic Rossby wave source that results from decomposition into barotropic and baroclinic components. Diagnoses using the NCEP-NCAR reanalysis are supplemented by analysis of the response of a tropical atmospheric model of intermediate complexity to the NCEP-NCAR barotropic Rossby wave source. Among the three barotropic Rossby wave source contributions (shear advection, vertical advection and surface drag), the leading contribution is from shear advection, and more specifically, the mean baroclinic zonal wind advecting the anomalous baroclinic zonal wind. Vertical advection is the smallest term, while surface drag tends to cancel and reinforce the shear advection in different regions through damping on baroclinic mode, which spins up a barotropic response. There are also non-trivial impacts of transients in the barotropic wind response to ENSO. Both tropical and subtropical baroclinic vorticity advection contribute to the barotropic component of the Pacific subtropical jet near coast of North America, where the resulting barotropic wind contribution approximately doubles the zonal jet anomaly at upper levels, relative to the baroclinic anomalies alone. In this view, the barotropic Rossby wave source in the subtropics simply arises from the basic-state baroclinic flow acting on the well-known baroclinic ENSO flow pattern that spreads from the deep tropics into the subtropics over a scale of equatorial radius of deformation. This is inseparably connected to the leading deep tropical Rossby wave source that arises from eastern Pacific climatological baroclinic winds advecting the tropical portion of the same ENSO flow pattern.

1. Introduction

Teleconnections from the ENSO heating region into midlatitudes are largely barotropic (Horel and Wallace 1981; Hoskins and Karoly 1981; Simmons 1982; Branstator 1983; Simmons et al. 1983; Held and Kang 1987) because barotropic modes can propagate to high turning latitudes. However, the tropical heat source associated with ENSO does not directly force a barotropic response. In the central and eastern tropical Pacific, ENSO is associated with tropospheric temperature anomalies that can be well described by baroclinic equatorial wave dynamics, with the response to heating tending to approximately resemble a baroclinic Rossby wave straddling the equator and a Kelvin wave at the equator (Kiladis and Diaz 1989; Wallace et al. 1998; Chiang and Sobel 2002; Su and Neelin 2002; Kumar and Hoerling 2003). Interactions between baroclinic and barotropic modes then force the barotropic Rossby wave trains that dominate the ENSO teleconnections in the North Pacific and North America.

In view of the vertical structure of teleconnections into midlatitudes, pure barotropic models have been widely used for their study (e.g., Hoskins and Karoly 1981; Simmons 1982; Simmons et al. 1983; Held and Kang 1987). Applications of this methodology, however, typically have prescribed a vorticity source or "Rossby wave source" (Sardeshmukh and Hoskins 1988). The prescribed source can be based, for instance, on the specification of baroclinic divergence at upper levels or on baroclinic transient motions diagnosed from a GCM simulation (Held and Kang 1987). Many components of a fixed source in this approach come from dynamical processes whose scales, spatial form, and so on depend on the interaction of the baroclinic mode with the basic state in ways that can be interesting to elucidate.

The motivation of our work is to investigate the complex baroclinic-to-barotropic pathway in the tropics to midlatitudes teleconnection process through baroclinic-barotropic interactions dur-

ing ENSO. In the equation for the barotropic component of the flow, the interactions with the baroclinic component are formally similar to the term traditionally described as a Rossby wave source, but their structure can be quantitatively and conceptually quite different than those based on upper-level divergent flow. For instance, if there is no vertical shear and no damping on the baroclinic mode associated with surface stress, then upper level divergence in the baroclinic mode does not produce any linear forcing of the barotropic mode. At the same time, by explicitly modeling the gravest baroclinic mode, the teleconnection pathway can be followed as the two modes interact. To maintain consistency with the earlier literature while emphasizing the systematic projection on the barotropic mode, the term "barotropic Rossby wave source" is used here. This is a shorthand for "baroclinic-barotropic interaction terms in the barotropic vorticity equation". Potential caveats on viewing these terms as a fixed source/sink of barotropic vorticity will be provided in discussion of the results, while arguing for the usefulness of the RWS as a diagnostic of the pathway between direct baroclinic response to SST in the tropics and the barotropic contribution to the response.

Multilevel linear, steady-state wave models with both baroclinic and barotropic components (Hoskins and Karoly 1981; Ting and Held 1990; DeWeaver and Nigam 2004) can capture at least some aspects of the tropical/baroclinic - midlatitude/barotropic transition. Held et al. (1985) show how a geostrophic barotropic mode is modified to an external mode in presence of shear, as further discussed in section 2b. Lee et al. (2009) use a simple two-level model to analyze the interaction of baroclinic and barotropic components in response to ENSO-like heating, as well as the importance of vertical background wind shear in exciting the barotropic response in midlatitudes. Majda and Biello (2003) emphasize the central role of baroclinic mean shear for sufficiently rapid nonlinear exchange of energy between the tropics and midlatitudes. Biello and Majda (2004a) explain how the dissipative mechanisms arising from radiative cooling and atmospheric boundary layer drag,

creates barotropic/baroclinic spinup/spindown in the teleconnection process. Interactions with baroclinic transient eddies (Held et al. 1989; Hoerling and Ting 1994; Straus and Shukla 1997) also alter the teleconnection pattern in a manner that is not easily captured by stationary wave models.

Our focus in the present study is on the forcing of the midlatitude barotropic response to ENSO by three barotropic-baroclinic interaction processes: (1) shear advection (Wang and Xie 1996; Neelin and Zeng 2000; Majda and Biello 2003; Biello and Majda 2004b; Lee et al. 2009), (2) surface drag (Neelin and Zeng 2000; Biello and Majda 2004a), and (3) vertical advection (Neelin and Zeng 2000; Bacmeister and Suarez 2002). Recently, Ji et al. (2014) analyzed in detail the roles that these three terms play in interhemispheric teleconnections from tropical heat sources. Moreover, Ji et al. (2015) examined the effects of these three terms in generating the sea level pressure anomalies in the western Pacific during El Niño, which are integral part of the Southern Oscillation pattern. Here, we examine the ENSO composites of baroclinic-barotropic interaction terms [the barotropic "Rossby wave source" (RWS)] calculated from NCEP-NCAR reanalysis. The NCEP RWS is then prescribed in the barotropic vorticity equation of a quasi-equilibrium tropical circulation model (QTCM, see model description in section 2c) used in previous studies to perform a set of diagnostic experiments. The barotropic teleconnection responses in these experiments are then compared to ENSO composites of the NCEP-NCAR reanalysis winds.

The remainder of the text is organized as follows. Section 2 gives a brief introduction of the datasets, model and methodology used in this study. Section 3 presents ENSO composite anomalies of tropospheric temperature, and of the baroclinic and barotropic components of wind, based on data from the NCEP-NCAR reanalysis. Section 4 presents the results of QTCM experiments in response to ENSO composite anomalies of the barotropic "Rossby wave source" — the baroclinic-

barotropic interaction terms — computed using NCEP-NCAR reanalysis, and further analysis of the dominant component of Rossby wave source. Section 5 consists of a summary and discussion.

2. Datasets, Model and Methodology

a. Datasets

We use monthly mean air temperature, zonal and meridional winds from NCEP-NCAR reanalysis (Kalnay et al. 1996), which covers the period from 1948 to the present date. Using this dataset we created composite plots corresponding to 6 El Niño events (1982-1983, 1986-1987, 1991-1992, 1997-1998, 2002-2003, and 2009-2010).

b. The barotropic Rossby wave source

The hydrostatic equation in pressure coordinates, $\partial_p \phi = -RT/p$, can be expressed in vertical integral form as:

$$\phi = \int_p^{p_r} RT\, d\ln p + \phi_r \tag{1}$$

where ϕ is the geopotential at pressure level p, T is temperature, R is the gas constant for air, p_r is a reference pressure, and ϕ_r is the geopotential on that pressure surface. The momentum equation of the primitive equations combined with the hydrostatic equation can be written as:

$$\begin{aligned} &(\partial_t + \mathbf{v}\cdot\nabla + \omega\partial_p - K_H\nabla^2)\mathbf{v} + f\mathbf{k}\times\mathbf{v} + g\partial_p\tau \\ &= -\nabla\textstyle\int_p^{p_r} RT\, d\ln p - \nabla\phi_r \end{aligned} \tag{2}$$

where $\mathbf{v}$ is horizontal velocity, ω is vertical velocity in pressure coordinates, K_H is the horizontal diffusion coefficient, f is the Coriolis parameter, τ is vertical flux of horizontal momentum, and g is gravitational acceleration.

The barotropic component of the flow is defined as a vertical average in the troposphere, $\langle X \rangle = p_T^{-1} \int_{p_{rt}}^{p_{rs}} X dp$, where p_{rs} and p_{rt} are pressure at the near-surface and tropopause reference levels, respectively (here, 1000 and 200 hPa, respectively), and $p_T = p_{rs} - p_{rt}$, and is denoted with subscript "0". Taking a vertical average of (2) yields:

$$\begin{aligned} &\partial_t \mathbf{v_0} + \mathbf{v_0} \cdot \nabla \mathbf{v_0} - K_H \nabla^2 \mathbf{v_0} + f\mathbf{k} \times \mathbf{v_0} + \nabla \phi_0 \\ &= -\langle \mathbf{v_1} \cdot \nabla \mathbf{v_1} \rangle - \langle (\nabla \cdot \mathbf{v_1}) \mathbf{v_1} \rangle - (g/p_T)\tau_s \end{aligned} \tag{3}$$

where the subscript "1" denotes the baroclinic component, which is defined as the deviation from the vertical mean and is a function of p. For simplicity, in the applications here where we are examining usefulness for ENSO anomalies, the effect of topography in the vertical integrals is omitted.

Taking $curl_z$ of (3), the anomaly equation for the barotropic stream function ψ_0 is, denoting anomalies relative to long-term mean climatology by prime:

$$\begin{aligned} &\partial_t \nabla^2 \psi_0{}' + curl_z(\mathbf{v}_0 \cdot \nabla \mathbf{v}_0)' + \beta v_0{}' - K_H \nabla^4 \psi_0{}' + curl_z(\varepsilon_0 \mathbf{v}_0)' \\ &= -\langle curl_z(\mathbf{v}_1 \cdot \nabla \mathbf{v}_1)' \rangle - \langle curl_z[(\nabla \cdot \mathbf{v}_1)\mathbf{v}_1]' \rangle - curl_z(\varepsilon_1 \mathbf{v}_{1s})' \end{aligned} \tag{4}$$

where β is the meridional derivative of the Coriolis parameter, $(g/p_T)\tau_s$ is parameterized by $(\varepsilon_0 \mathbf{v}_0 + \varepsilon_1 \mathbf{v}_{1s})$, with $\varepsilon_0 = \varepsilon_1 = (g/p_T)\rho_a C_D V_s$, and where ρ_a is the near-surface air density, C_D is the drag coefficient, V_s is the near-surface wind speed. Note that all terms that involve the barotropic component of the flow have been placed on the lhs of (4). The terms on the rhs of (4) act as a barotropic Rossby wave source, which acts to excite the barotropic mode in a manner akin to well-known studies of barotropic teleconnections reviewed in the Introduction section of this paper (Hoskins and Karoly 1981; Held and Kang 1987; Sardeshmukh and Hoskins 1988). We emphasize that this is noticeably different than the Rossby wave source that would be defined by assuming an upper-level forcing applied to the barotropic mode, because it results from a repre-

sentation of the modal breakdown over the full depth of the troposphere (Neelin and Zeng 2000; Majda and Biello 2003). If one considers a linearization of (4) about a basic state with no baroclinic mean wind or surface damping, the barotropic mode is a free solution, separated from the baroclinic modes. Held et al. (1985) show that in presence of horizontally constant shear, a solution can be obtained for an external mode that is closely related to the barotropic mode but with some baroclinic contributions. These contributions vanish as the basic state shear goes to zero. A barotropic vorticity equation with an assumed Rossby wave source containing an upper-level divergence term does not capture this dependence on shear. In the approximation here, the vertical velocity interaction with shear is seen as one term in the barotropic Rossby wave source.

Interpreting the individual terms on the rhs of (4), the contributions of baroclinic-barotropic interaction in such a barotropic Rossby wave source are: (1) $-\langle curl_z(\mathbf{v}_1 \cdot \nabla \mathbf{v}_1)' \rangle$, representing the horizontal advection processes; (2) $-\langle curl_z[(\nabla \cdot \mathbf{v}_1)\mathbf{v}_1]' \rangle$, representing vertical advection processes; (3) $-curl_z(\varepsilon_1 \mathbf{v}_{1s})'$, representing surface drag processes. Ji et al. (2014) analyzed the effects of each mechanism on forcing barotropic mode and associated teleconnection pathways from a tropical heat source. Ji et al. (2015) further examined the effects of each mechanism on the sea level pressure anomalies in the western Pacific during ENSO events.

For some purposes it can be useful to expand the anomaly terms as products of long-term climatology terms denoted with overbar and ENSO anomaly terms denoted with prime. Equation (4)

then becomes

$$
\begin{aligned}
&\partial_t \nabla^2 \psi_0{}' + curl_z(\bar{\mathbf{v}}_0 \cdot \nabla \mathbf{v}_0{}') + curl_z(\mathbf{v}_0{}' \cdot \nabla \bar{\mathbf{v}}_0) \\
&+ curl_z(\overline{\mathbf{v}_0{}' \cdot \nabla \mathbf{v}_0{}'}) + T_0' \\
&+ \beta v_0{}' - K_H \nabla^4 \psi_0{}' + curl_z(\varepsilon_0 \mathbf{v}_0)' \\
&= -\langle curl_z(\bar{\mathbf{v}}_1 \cdot \nabla \mathbf{v}_1{}')\rangle - \langle curl_z(\mathbf{v}_1{}' \cdot \nabla \bar{\mathbf{v}}_1)\rangle \\
&- \langle curl_z[(\nabla \cdot \bar{\mathbf{v}}_1)\mathbf{v}_1{}']\rangle - \langle curl_z[(\nabla \cdot \mathbf{v}_1{}')\bar{\mathbf{v}}_1]\rangle \\
&- \left\langle curl_z(\overline{\mathbf{v}_1{}' \cdot \nabla \mathbf{v}_1{}'})\right\rangle - \left\langle curl_z[\overline{(\nabla \cdot \mathbf{v}_1{}')\mathbf{v}_1{}'}]\right\rangle \\
&- curl_z(\varepsilon_1 \mathbf{v}_{1s})' - T_1'
\end{aligned}
\tag{5}
$$

Because the ENSO anomaly terms represent averages over a specific set of months with ENSO conditions (e.g. a composite of Dec.-Feb. over a set of El Niño years) minus the long-term climatological average, there will also be contributions from nonlinear interactions of transient motions at shorter timescales over the ENSO conditional average minus their climatological average. These transient term anomalies are denoted T_0' where they arise from nonlinear interaction between barotropic terms on the LHS of (5), and are denoted T_1' where they arise from nonlinear interaction between baroclinic terms on the RHS. From previous work indicating substantial changes in transients during El Niño (Held et al. 1989; Hoerling and Ting 1994; Straus and Shukla 1997), we can anticipate that these will not be small terms in the budget. However, the baroclinic changes within the tropics that initiate the set of interactions being diagnosed here are widely modeled as an approximately steady-state response to ENSO SST forcing. It is thus reasonable to first diagnose the baroclinic-barotropic interactions represented by the climatology-ENSO anomaly interaction terms explicitly broken out on the RHS of (5)—this will be the focus of the present study. This sets up the first-step stationary wave pattern that would then interact with mid-latitude storm tracks. Although this difficult transient interaction problem is not modeled here, the magnitude of the problem can be estimated by evaluating residuals from the explicit terms in the barotropic

vorticity budget (5). This provides an estimate of $-(T_0+T_1)$ plus any errors from the spatial finite differencing of the reanalysis fields.

Depending on the problem being addressed, the barotropic RWS could be defined to include transient terms. For purposes here, the discussion is more compact if we define it as the explicit terms on the RHS of (5) when we are breaking out individual terms. For simplicity of computation when terms are not broken out, we use the RHS of (4) evaluated with monthly average data, which is numerically extremely close. In diagnosing the most important anomaly terms, the shear advection contribution to the barotropic Rossby Wave Source anomaly RWS$'$ can be approximately broken out as

$$\begin{aligned}\mathrm{RWS}'_{shear} = &-\langle curl_z(\bar{\mathbf{v}}_1\cdot\nabla\mathbf{v}_1{}')\rangle - \langle curl_z(\mathbf{v}_1{}'\cdot\nabla\bar{\mathbf{v}}_1)\rangle \\ &-\left\langle curl_z(\overline{\mathbf{v}_1{}'\cdot\nabla\mathbf{v}_1{}'})\right\rangle \\ \approx &\frac{\partial}{\partial y}\left\langle \bar{u}_1\frac{\partial u_1{}'}{\partial x}+\bar{v}_1\frac{\partial u_1{}'}{\partial y}\right\rangle + \frac{\partial}{\partial y}\left\langle u_1{}'\frac{\partial \bar{u}_1}{\partial x}+v_1{}'\frac{\partial \bar{u}_1}{\partial y}\right\rangle \\ &-\frac{\partial}{\partial x}\left\langle \bar{u}_1\frac{\partial v_1{}'}{\partial x}+\bar{v}_1\frac{\partial v_1{}'}{\partial y}\right\rangle - \frac{\partial}{\partial x}\left\langle u_1{}'\frac{\partial \bar{v}_1}{\partial x}+v_1{}'\frac{\partial \bar{v}_1}{\partial y}\right\rangle\end{aligned} \tag{6}$$

of which the first term gives the leading approximation. Similarly the vertical advection contribution can be approximately broken out as

$$\begin{aligned}\mathrm{RWS}'_{vert} = &-\langle curl_z[(\nabla\cdot\bar{\mathbf{v}}_1)\mathbf{v}_1{}']\rangle - \langle curl_z[(\nabla\cdot\mathbf{v}_1{}')\bar{\mathbf{v}}_1]\rangle \\ &-\left\langle curl_z[\overline{(\nabla\cdot\mathbf{v}_1{}')\mathbf{v}_1{}'}]\right\rangle \\ \approx &\frac{\partial}{\partial y}\left\langle (\frac{\partial u_1{}'}{\partial x}+\frac{\partial v_1{}'}{\partial y})\bar{u}_1\right\rangle + \ldots\end{aligned} \tag{7}$$

Finally, vorticity source terms tend to emphasize small scales, which can be distracting for visualizing components that are important to the large-scale stationary wave response. One common approach is to filter with an inverse Laplacian, but this tends to over-emphasize the larger scales. We use two approaches to addressing this visualization problem. The primary approach is to display the RWS anomaly as a vorticity source, but then to also display the response of an intermediate complexity model to the RWS, as discussed in Section 2c. As a secondary method

specifically for the discussion of leading terms in (6) and (7), we display terms both with and without taking the curl. For zonally elongated features such as the El Niño subtropical jet anomalies in the Eastern Pacific that are of particular interest here, this corresponds to diagnosing the zonal acceleration term, similar to the approach used by Straus and Shukla (1997).

c. QTCM

The QTCM belongs to a class of tropical atmospheric models of intermediate complexity that occupies a niche between GCMs and simple models. The model takes analytical solutions that hold approximately under quasi-equilibrium (QE) conditions and employs them as leading basis functions to represent the vertical structure of the flow. The primitive equations are then projected onto these simplified vertical structures, with self-consistent nonlinear terms retained in advection, moist convection, and vertical momentum transfer terms, among others. A more detailed model description can be found in Neelin and Zeng (2000). The QTCM has been used to analyze the moist dynamics of ENSO teleconnections in a number of contexts (Su et al. 2001, 2003, 2005; Neelin and Su 2005; Lintner and Chiang 2007).

The present study uses the first generation QTCM (QTCM1), version 2.3. This version retains a single basis function for the vertical structure of temperature, with two components in the vertical structure of velocity: barotropic V_0 and baroclinic V_1, where the subscript 0 refers to the barotropic mode that is vertically independent to horizontal temperature variations, which has the same form as (4); and the subscript 1 refers to a single deep baroclinic mode corresponding to the vertical structure of temperature in the QTCM. Note the slight difference with the notation used in the previous section, where the subscript 1 referred to the baroclinic contribution that can have any vertical structure. A more detailed description of the QTCM equations is given in the appendix.

We perform several experiments with the QTCM to analyze the pathway of atmospheric teleconnections in the Pacific from tropical ENSO heating to the mid- and high latitudes. In these experiments, the ENSO December-February (DJF) composite anomalies of monthly baroclinic-barotropic interaction terms are used as the forcing, instead of ENSO SST anomalies. Then the barotropic teleconnections in response to those interaction terms are compared to the teleconnection patterns calculated as the ENSO composite anomalies in NCEP-NCAR reanalysis. These experiments provide a way of interpreting the large-scale barotropic wave response to ENSO forced by those baroclinic-barotropic interactions. Although we keep the barotropic-to-baroclinic feedback in the QTCM, the results here should be reproduced using a pure barotropic model. The caveats are that as waves propagate far from the source, the accurate simulation of background zonal wind becomes essential. The QTCM uses its own background field, which is shown below (Fig. 1) to have good agreement with that from NCEP-NCAR reanalysis. Due to model limitations in simulating the basic state, we should not completely trust the far field response, however, the wave response close to the source in this self-consistent baroclinic-barotropic decomposition model should compare reasonably well with that from NCEP-NCAR reanalysis and other models prescribing the reanalysis background winds.

Figure 1 shows the DJF mean climatology of barotropic zonal wind and baroclinic zonal wind at 200mb from the NCEP-NCAR reanalysis and a 100-year QTCM run with climatological SSTs. Recall that the barotropic component is independent of p, and is represented as the vertical mean in NCEP-NCAR reanalysis. The baroclinic component is calculated as the departures from vertical mean at each level. We choose to present 200mb baroclinic wind because this level is important for steering storms that impact the California coast during ENSO, and is also a typical level selected for representing the basic state flow in previous studies using simpler barotropic models. The most noticeable feature in Fig. 1 is that the barotropic and baroclinic components reinforce each

other in the subtropical jet region in the Northern Pacific. The background winds generally agree well between the reanalysis and model simulation, in regards to the jet location in western Pacific, the extended easterlies in the tropics, as well as the westerlies in the subtropical North Atlantic, although the jet has a broader structure in the NCEP-NCAR reanalysis compared to the model simulations.

3. ENSO composites in the NCEP-NCAR reanalysis

Figure 2 shows ENSO DJF composite anomalies of the tropospheric temperature and baroclinic vector wind at 200mb from NCEP-NCAR reanalysis. The most prominent feature of these temperature anomalies is consistent with a baroclinic Rossby wave straddling the equator in the eastern Pacific and a Kelvin wave-like structure extending to the east. There are also statistically significant temperature anomalies in the North Pacific and North America region. The baroclinic wind anomalies at 200mb are roughly consistent with geostrophic thermal wind balance in the subtropics and midlatitudes. The baroclinic shear advecting the baroclinic wind anomalies in both tropics and subtropics force the barotropic response in ENSO teleconnections, which we will discuss in further detail in Fig. 4.

Figure 3 shows ENSO DJF composite anomalies of upper-level (200mb) and lower-level (1000mb) zonal winds and their baroclinic components from NCEP-NCAR reanalysis. The upper-level easterlies on the equator in 200mb zonal wind, together with the lower level westerlies in 1000mb zonal wind, indicate a dominant baroclinic structure in the deep tropics. In the subtropical Pacific, the wind anomalies associated with ENSO have a substantial barotropic component, indicated by anomalous westerlies throughout the troposphere in 200mb and 1000mb winds. In the subtropics and midlatitudes, at 1000mb, the barotropic contribution to the surface wind (Fig.

4) cancels the baroclinic contribution (Fig. 3d) to a large extent, as one would expect when surface drag is effective at reducing the near-surface wind, and spinning up a strong barotropic component.

Figure 4 shows ENSO DJF composite anomalies of barotropic zonal wind from NCEP-NCAR reanalysis. The barotropic component is substantial in the subtropics where the subtropical jet extends between 20°N-30°N off the U.S coast, with a magnitude similar to the baroclinic component (Fig. 3b). The barotropic contribution in the tropics is also non-negligible.

4. The barotropic RWS and QTCM experiments

Figure 5 shows ENSO DJF composite anomalies of the barotropic RWS (Fig. 5a) [i.e., the rhs of (4)], together with each of the three components: shear advection (Fig. 5b), vertical advection (Fig. 5c), and surface drag (Fig. 5d) from NCEP-NCAR reanalysis. Figure 5e shows the residual calculated by subtracting the barotropic RWS from $curl_z(\mathbf{v}_0 \cdot \nabla \mathbf{v}_0) + \beta v_0$, and Fig. 5f is sum of the barotropic RWS and the residual. Because the curl is taken in the barotropic RWS terms, many small-scale features are present due to the spatial derivative. However, the barotropic wind (or stream function) response will appear primarily on scales of the stationary Rossby wavelength, roughly a few thousand kilometers (estimated using $2\pi\sqrt{\frac{u_0}{\beta}}$ with u_0 around 30 m s^{-1}, and β on the order of 10^{-11} m^{-1} s^{-1}). To better visualize the response, it is useful to have a model result forced by these RWS terms, for which we use the QTCM. The box indicates the Pacific region where the forcing is applied in the QTCM experiments, values outside the region is set to zero.

We next present results from pairs of 100-year QTCM simulations: one is the control or climatological run and the other is performed with ENSO DJF composite anomalies of each forcing source in Fig. 5 added to the rhs of the barotropic vorticity equation (RWS run). Both runs use monthly-mean climatological SSTs. Differences between each pair are thus due to the response to

each forcing anomalies within the Pacific region. The 100-year simulation length is used to obtain statistically significant results.

Figure 6 shows the QTCM DJF barotropic wind anomalies in response to each forcing source in Fig. 5. The barotropic wind response to the barotropic RWS show qualitatively good agreement with the DJF composite anomalies of barotropic wind from NCEP-NCAR reanalysis in Fig. 4, in the tropical central Pacific, the subtropical northern Pacific and the North America region. The contributions from each of the three baroclinic-barotropic interaction terms are not negligible, and they alternately cancel and reinforce each other in different regions. That being said, the vertical advection contribution is noticeably smaller among the three, even in the tropics. This is in contrast to traditional assumptions that upper-level divergence is an important forcing term. The shear advection contribution is larger among the three, modified by the other two sources, especially by surface drag in the western Pacific. In the region off California coast, where the subtropical jet extends further east in ENSO, the three interaction terms reinforce each other. For the case of residual forcing shown in Fig. 6e, there is a substantial response off the U.S. coast. Lastly, in Fig. 6f, we show the barotropic wind response to the sum of the barotropic RWS and the residual. In this case, the response off U.S. coast is qualitatively similar to the case forced by the barotropic RWS in Fig. 6a, with a larger amplitude.

While we have to be cautious about the residual calculation since it can include finite differencing errors, a leading contribution is presumed to be due to the nonlinear effects of departures from the monthly averages due to high-frequency storm transients, $-(T_0 + T_1)$ in (5). Reinforcement of the ENSO subtropical to mid-latitude anomalies by changes in storm statistics has previously been noted (Held et al. 1989; Hoerling and Ting 1994; Straus and Shukla 1997). The residual term in Fig. 5e is generally consistent with the existing hypothesis that the ENSO response in the deep tropics is reasonably modeled by a steady-state atmospheric response, which then modifies

the storm track at the subtropical/mid-latitude boundary, especially in the Eastern Pacific in the winter hemisphere. The wave-mean flow interaction with the transients is hypothesized to occur by steering baroclinic storms further toward the Eastern Pacific, and the radiated high-frequency Rossby waves provide an eastward momentum flux back into the jet (Straus and Shukla 1997). The jet anomalies in the subtropics can thus be interpreted as a substantial contribution from the monthly mean RWS, reinforced by associated changes in transients. In this respect, the RWS in the subtropics should be regarded as a diagnostic for the feedback, rather than a fixed source, although the results are consistent with initiation by steady response in the tropics. Here we can see that the feedback of the transients is strong in the Eastern subtropical Pacific in a systematic projection on the barotropic mode, and that both baroclinic and barotropic ENSO anomaly contributions are important in the subtropical jet changes.

We now turn to the key stage of the tropical-to-subtropical, baroclinic-barotropic interaction by breaking down contributions of the RWS anomaly. To identify the dominant component of shear advection forcing, we examine each of the four components of the the linearization (6). We find the largest component is the first term $\frac{\partial}{\partial y}\left\langle \bar{u}_1 \frac{\partial u_1{}'}{\partial x} + \bar{v}_1 \frac{\partial u_1{}'}{\partial y} \right\rangle$, which is shown in Fig. 7a. To assist in visualization and interpretation, as discussed in Section 2b, Figure 7b shows the same term as in Fig. 7a, but without the curl, as it appears in $u_0{}'$ equation, i.e., $\partial_t u_0{}' = -\left\langle \bar{u}_1 \frac{\partial u_1{}'}{\partial x} + \bar{v}_1 \frac{\partial u_1{}'}{\partial y} \right\rangle + \ldots$. Without the curl, the same term shows slightly larger spatial scales and shifted maximum and minimum locations. Figures 7c and 7d show $\left\langle \bar{u}_1 \frac{\partial u_1{}'}{\partial x} \right\rangle$ and $\left\langle \bar{v}_1 \frac{\partial u_1{}'}{\partial y} \right\rangle$ respectively. The mean baroclinic zonal wind advecting the anomalous baroclinic zonal wind $\left\langle \bar{u}_1 \frac{\partial u_1{}'}{\partial x} \right\rangle$ is the larger of the two, the pattern of which coincides well with barotropic wind response to shear advection in Fig. 6b. In the subtropics, baroclinic $\bar{u}_1$ at 200mb (Fig. 1b) advecting positive $\frac{\partial u_1{}'}{\partial x}$ (Fig. 2) results in the large positive area in the subtropical jet region in Fig. 7c. Similarly, the negative area east of the positive area close to the U.S. coast is due to the negative $\frac{\partial u_1{}'}{\partial x}$ (Fig. 2) in that region. The large

positive region in the tropical eastern Pacific appears because of the modest $\bar{u}_1$ at 200mb (Fig. 1b) advecting strong positive gradient $\frac{\partial u_1{}'}{\partial x}$ (Fig. 2). For the meridional case in Fig. 7d, the two negative regions result from modest values of $\bar{v}_1$ (not shown) advecting large gradient $\frac{\partial u_1{}'}{\partial y}$ (Fig. 2). The same analysis applies at lower levels with sign reversed for both mean and anomalies, which gives the forcing in the same direction.

If we assume that the response to the barotropic RWS is approximately linear, we can explore how large the contribution is from different regions. We perform two experiments with the barotropic RWS in two narrower boxes: one is in tropics (15°N-15°S, 160°E-80°W); the other is in subtropics (15°N-40°N, 160°E-100°W). We find that off the U.S. coast, roughly half of the jet response is due to forcing in the subtropics locally, and half is due to forcing in the tropics (figures not shown). From the previous analysis on shear advection decomposition, it is easy to see that while such experiments are easy to do, and may help to understand the relative contribution of different parts of the Rossby wave source, the separation into tropics and subtropics is artificial. The barotropic teleconnections in the subtropical jet region result from the basic state baroclinic wind advection acting on the baroclinic response to ENSO seen in the flow pattern in Fig. 2, which spreads by baroclinic wave dynamics from the deep tropics into subtropics on the scale of equatorial radius of deformation. Figure 8 illustrates some aspects of this interaction. The baroclinic response spreads from the ENSO heating to yield the characteristic baroclinic stationary wave pattern in the tropics and subtropics. At particular locations, the climatological baroclinic shear interacts strongly with this anomalous ENSO pattern, yielding the barotropic Rossby wave source that projects on the barotropic component. The response to this plus surface drag contributions yields the barotropic contribution to the ENSO response. Rather than assuming a forcing by the sensitive divergent component of the flow, diagnosing the pathway under this view emphasizes the

role of the baroclinic dynamics in setting up the ENSO anomaly, and puts the focus on interactions of these anomalous winds patterns with surface drag and the basic state shear.

Similarly with what we did for shear advection, we examine the linearization of the vertical advection term (7), and identify the dominant component as $\frac{\partial}{\partial y}\left\langle (\frac{\partial u_1{}'}{\partial x} + \frac{\partial v_1{}'}{\partial y})\bar{u}_1 \right\rangle$ shown in Fig. 9a. Figure 9b shows the same term without the curl: $\left\langle (\frac{\partial u_1{}'}{\partial x} + \frac{\partial v_1{}'}{\partial y})\bar{u}_1 \right\rangle$. The ingredients of this vertical advection term may be seen from the anomalous vertical velocity $\langle \omega' \rangle$ (Fig. 9c, with negative values corresponding to upper level divergence) advecting the mean baroclinic shear $\bar{u}_1$ (Fig. 1b). The positive and negative forcing in Fig. 9b comes from the corresponding anomalous ascending and descending motion (Fig. 9c), but it is strongly weighted by the basic-state shear (Fig. 1b) in different regions. As a result, the strong equatorial vertical velocity anomalies yield only weak contributions, and the main barotropic RWS vertical advection contributions come from the subtropics in the region of strong baroclinic jet. It may also be noted that along the equator in the Indian ocean/maritime continent region, the different sign of the shear affects the sign of this contribution. Overall, however, the key point is that the contribution of upper-level divergence anomalies, which had been a focus of prior studies, tends to be smaller than that of the other terms.

5. Conclusions

To understand the complex baroclinic-to-barotropic pathway in the tropical to midlatitude ENSO teleconnection process, it can be useful to examine an approach that considers a systematic modal breakdown of baroclinic and barotropic modes. In this view, the barotropic mode is forced by the baroclinic-barotropic interaction terms, which yield the barotropic Rossby wave source. These RWS interaction terms are diagnosed from the NCEP-NCAR reanalysis data to create ENSO anomalies. Different from the classic studies that assume that a diagnosed upper-level vorticity

source forces a barotropic mode, the barotropic RWS in our approach represents the forcing on the barotropic component evaluated through the atmospheric column (here 200mb to the surface). Under these approximations, baroclinic and barotropic components of ENSO wind anomalies are examined as composites from the NCEP-NCAR reanalysis. The barotropic component is substantial even in the tropical Pacific, implying that a purely baroclinic mode representation of ENSO would be incomplete even within the forcing region. In the subtropical Pacific off the U.S. west coast, which can be important for ENSO impacts on North America, the baroclinic contribution remains substantial, but the barotropic mode contribution doubles the subtropical jet response to ENSO.

Composite ENSO anomalies of the barotropic RWS as vorticity source contributions that appear on the r.h.s of barotropic vorticity equation can be interpreted directly, but it can also be useful to see the associated wind solutions. For this, the QTCM, a model with an explicit baroclinic barotropic mode breakdown, is used to diagnose the response. In these QTCM experiments, the barotropic vorticity equation of the model is forced by the composite ENSO anomaly barotropic RWS diagnosed from the NCEP-NCAR reanalysis. The resulting zonal wind anomalies (compared to the wind in a control run) are qualitatively in good agreement with those of the ENSO composite barotropic wind response from the NCEP reanalysis, including in the subtropics off the U.S. coast. Although there are non-trivial impacts of transients in the barotropic wind response to ENSO, qualitatively, the barotropic response near coast of North America is set up by the barotropic Rossby wave source term as diagnosed from monthly means for ENSO anomaly composite response. Among the three barotropic Rossby wave source contributions (shear advection, vertical advection and surface drag), vertical advection contributions arise from anomalous vertical velocity in regions where there is climatological baroclinic shear, but these terms tend to be smaller than the others. This is in contrast to traditional assumptions that upper-level di-

vergence is an important forcing term. The surface drag contribution alternately tends to cancel or reinforce the shear advection in different regions through damping on baroclinic mode which spins up a barotropic response. The dominant contributions are from the shear advection. Further decomposition of the shear advection term shows that the mean baroclinic zonal wind advecting the anomalous baroclinic zonal wind is the most import component. Shear advection in both the tropics and subtropics contribute to the subtropical response, but both are an integral part of basic state advection of the baroclinic ENSO flow pattern. In this view, the barotropic Rossby wave source in the subtropics simply arises from the basic state baroclinic flow acting on the well-known baroclinic ENSO flow pattern that spreads from the deep tropics into the subtropics over a scale of equatorial radius of deformation. This is inseparably connected to the leading deep tropical Rossby wave source that arises from Eastern Pacific basic state baroclinic winds advecting the tropical portion of the same ENSO flow pattern.

Acknowledgments. This work was supported in part by National Science Foundation grant AGS-1540518 and AGS-1041477, and National Oceanic and Atmospheric Administration grant NA14OAR4310274. We thank J. Meyerson for graphical assistance.

APPENDIX

QTCM equations

In the QTCM, the momentum equation (2) is projected onto the barotropic and baroclinic wind vertical structures, i.e., using V_0 and V_1 as the basis functions, and taking the inner product of the momentum equation with V_0 and V_1 respectively. For the barotropic component:

$$\partial_t \mathbf{v_0} + D_{V0}(\mathbf{v_0},\mathbf{v_1}) + f\mathbf{k}\times\mathbf{v_0} + (g/p_T)\tau_s = -\nabla\phi_0 \tag{A.1}$$

with

$$D_{V0}(\mathbf{v_0},\mathbf{v_1}) = \mathbf{v_0}\cdot\nabla\mathbf{v_0} + \left\langle V_1^2\right\rangle \mathbf{v_1}\cdot\nabla\mathbf{v_1} + \left\langle V_1^2\right\rangle (\nabla\cdot\mathbf{v_1})\mathbf{v_1} - K_H\nabla^2\mathbf{v_0} \tag{A.2}$$

Taking a $curl_z$ of Eq. (A.1) yields the barotropic vorticity equation similar to Eq. (4) in the main text. The baroclinic wind component is governed by:

$$\partial_t \mathbf{v}_1 + D_{V1}(\mathbf{v_0},\mathbf{v_1}) + f\mathbf{k}\times\mathbf{v}_1 + g\left\langle V_1^2\right\rangle^{-1}\left\langle V_1\partial_p\tau\right\rangle = -\kappa\nabla T_1 \tag{A.3}$$

where $D_{V1}(\mathbf{v_0},\mathbf{v_1})$ is the advection-diffusion operator similar to (A.2) but for the baroclinic wind component. In the QTCM experiments in the main text, only the barotropic equation is forced by the barotropic RWS. However, because of the baroclinic-barotropic interaction terms in Eq. (A.3), there will be a baroclinic response (see Fig. A1) in these experiments arising from the self-consistent baroclinic-barotropic decomposition. In other words, the QTCM simulates an external mode response in which the barotropic solution has an associated small baroclinic contribution via the baroclinic-barotropic interaction terms.

The geopotential gradient term $-\kappa\nabla T_1$ in Eq. (A.3) appears simple because $V_1(p)$ has been chosen to match the hydrostatic integral of the vertical structure of temperature, $a_1(p)$, with $\kappa = R/c_p$. The temperature coefficient, $T_1(x,y,t)$, is governed by the temperature equation for deep baroclinic structure:

$$\langle a_1\rangle(\partial_t + D_{T1})T_1 + M_{S1}\nabla\cdot\mathbf{v}_1 = \langle Q_c\rangle + \langle Q_R\rangle \tag{A.4}$$

where D_{T1} is the advection-diffusion operator for temperature, M_{S1} is the dry static stability for a vertical velocity profile derived from $V_1(p)$, and $\langle Q_c \rangle$ and $\langle Q_R \rangle$ are the vertical average convective and radiative plus sensible heating of the column. The convective heating is given by the convective parameterization that depends on temperature and moisture, with the moisture equation vertically projected on a single basis function (see Neelin and Zeng (2000) for details and other definitions). The driving by SST appears in the surface radiative and sensible heat fluxes that contribute to $\langle Q_R \rangle$ and in evaporation, as in a standard primitive equation model. The SST thus directly forces a prognostic baroclinic response in temperature, moisture and baroclinic wind. The barotropic response is forced by the baroclinic response through the interaction terms in (A.1), including surface drag and the baroclinic advection terms given by (A.2).

References

Bacmeister, J. T., and M. J. Suarez, 2002: Wind stress simulations and the equatorial momentum budget in an AGCM. *Journal of the Atmospheric Sciences*, **59 (21)**, 3051–3073.

Biello, J. A., and A. J. Majda, 2004a: Boundary layer dissipation and the nonlinear interaction of equatorial baroclinic and barotropic rossby waves. *Geophysical & Astrophysical Fluid Dynamics*, **98 (2)**, 85–127.

Biello, J. A., and A. J. Majda, 2004b: The effect of meridional and vertical shear on the interaction of equatorial baroclinic and barotropic rossby waves. *Studies in Applied Mathematics*, **112 (4)**, 341–390.

Branstator, G., 1983: Horizontal energy propagation in a barotropic atmosphere with meridional and zonal structure. *Journal of the Atmospheric Sciences*, **40 (7)**, 1689–1708.

Chiang, J. C. H., and A. H. Sobel, 2002: Tropical tropospheric temperature variations caused by ENSO and their influence on the remote tropical climate. *Journal of Climate*, **15 (18)**, 2616–2631.

DeWeaver, E., and S. Nigam, 2004: On the forcing of ENSO teleconnections by anomalous heating and cooling. *Journal of Climate*, **17 (16)**, 3225–3235.

Held, I. M., and I.-S. Kang, 1987: Barotropic models of the extratropical response to El Niño. *Journal of the Atmospheric Sciences*, **44 (23)**, 3576–3586.

Held, I. M., S. W. Lyons, and S. Nigam, 1989: Transients and the extratropical response to El Niño. *Journal of the Atmospheric Sciences*, **46 (1)**, 163–174.

Held, I. M., R. L. Panetta, and R. T. Pierrehumbert, 1985: Stationary external Rossby Waves in vertical shear. *Journal of the Atmospheric Sciences*, **42 (9)**, 865–883.

Hoerling, M. P., and M. Ting, 1994: Organization of extratropical transients during El Niño. *Journal of Climate*, **7 (5)**, 745–766.

Horel, J. D., and J. M. Wallace, 1981: Planetary-scale atmospheric phenomena associated with the Southern Oscillation. *Monthly Weather Review*, **109 (4)**, 813–829.

Hoskins, B. J., and D. J. Karoly, 1981: The steady linear response of a spherical atmosphere to thermal and orographic forcing. *Journal of the Atmospheric Sciences*, **38 (6)**, 1179–1196.

Ji, X., J. D. Neelin, S.-K. Lee, and C. R. Mechoso, 2014: Interhemispheric teleconnections from tropical heat sources in intermediate and simple models. *Journal of Climate*, **27 (2)**, 684–697.

Ji, X., J. D. Neelin, and C. R. Mechoso, 2015: El Niño/Southern Oscillation Sea Level Pressure anomalies in the western Pacific: Why are they there? *Journal of Climate*, **28 (22)**, 8860–8872.

Kalnay, E., and Coauthors, 1996: The NCEP/NCAR 40-year reanalysis project. *Bulletin of the American Meteorological Society*, **77 (3)**, 437–471.

Kiladis, G. N., and H. F. Diaz, 1989: Global climatic anomalies associated with extremes in the Southern Oscillation. *Journal of Climate*, **2 (9)**, 1069–1090.

Kumar, A., and M. P. Hoerling, 2003: The nature and causes for the delayed atmospheric response to El Niño. *Journal of Climate*, **16 (9)**, 1391–1403.

Lee, S.-K., C. Wang, and B. E. Mapes, 2009: A simple atmospheric model of the local and teleconnection responses to tropical heating anomalies. *Journal of Climate*, **22 (2)**, 272–284.

Lintner, B. R., and J. C. H. Chiang, 2007: Adjustment of the remote tropical climate to El Niño conditions. *Journal of Climate*, **20 (11)**, 2544–2557.

Majda, A. J., and J. A. Biello, 2003: The nonlinear interaction of barotropic and equatorial baroclinic Rossby waves. *Journal of the Atmospheric Sciences*, **60 (15)**, 1809–1821.

Neelin, J. D., and H. Su, 2005: Moist teleconnection mechanisms for the tropical south American and Atlantic sector. *Journal of Climate*, **18 (18)**, 3928–3950.

Neelin, J. D., and N. Zeng, 2000: A quasi-equilibrium tropical circulation model—formulation. *Journal of the Atmospheric Sciences*, **57 (11)**, 1741–1766.

Sardeshmukh, P. D., and B. J. Hoskins, 1988: The generation of global rotational flow by steady idealized tropical divergence. *Journal of the Atmospheric Sciences*, **45 (7)**, 1228–1251.

Simmons, A. J., 1982: The forcing of stationary wave motion by tropical diabatic heating. *Quarterly Journal of the Royal Meteorological Society*, **108 (457)**, 503–534.

Simmons, A. J., J. M. Wallace, and G. W. Branstator, 1983: Barotropic wave propagation and instability, and atmospheric teleconnection patterns. *Journal of the Atmospheric Sciences*, **40 (6)**, 1363–1392.

Straus, D. M., and J. Shukla, 1997: Variations of midlatitude transient dynamics associated with enso. *Journal of the Atmospheric Sciences*, **54**, 777–790.

Su, H., and J. D. Neelin, 2002: Teleconnection mechanisms for tropical pacific descent anomalies during El Niño. *Journal of the Atmospheric Sciences*, **59 (18)**, 2694–2712.

Su, H., J. D. Neelin, and C. Chou, 2001: Tropical teleconnection and local response to sst anomalies during the 1997–1998 El Niño. *Journal of Geophysical Research: Atmospheres*, **106 (D17)**, 20 025–20 043.

Su, H., J. D. Neelin, and J. E. Meyerson, 2003: Sensitivity of tropical tropospheric temperature to sea surface temperature forcing. *Journal of Climate*, **16 (9)**, 1283–1301.

Su, H., J. D. Neelin, and J. E. Meyerson, 2005: Mechanisms for lagged atmospheric response to ENSO SST forcing. *Journal of Climate*, **18 (20)**, 4195–4215.

Ting, M., and I. M. Held, 1990: The stationary wave response to a tropical SST anomaly in an idealized GCM. *Journal of the Atmospheric Sciences*, **47 (21)**, 2546–2566.

Wallace, J. M., E. M. Rasmusson, T. P. Mitchell, V. E. Kousky, E. S. Sarachik, and H. von Storch, 1998: On the structure and evolution of ENSO-related climate variability in the tropical Pacific: Lessons from TOGA. *Journal of Geophysical Research: Oceans*, **103 (C7)**, 14 241–14 259.

Wang, B., and X. Xie, 1996: Low-frequency equatorial waves in vertically sheared zonal flow. part i: Stable waves. *Journal of the Atmospheric Sciences*, **53 (3)**, 449–467.

LIST OF FIGURES

Fig. 1. DJF climatology of (a) NCEP barotropic zonal wind ($\bar{u}_0$), (b) NCEP baroclinic zonal wind at 200mb ($\bar{u}_{200}$-baroclinic), (c) $\bar{u}_0$ from a 100yr QTCM run with climatological SSTs, and (d) QTCM $\bar{u}_{200}$-baroclinic. The units are m s $^{-1}$. 28

Fig. 2. NCEP ENSO DJF composite anomalies of vertically averaged tropospheric temperature (T'_{avg}) and 200mb baroclinic wind (u'_{200}-baroclinic). The units are K for temperature, and m s^{-1} for winds. Shading denotes regions where the temperature anomaly passes a two-sided t-test at the 95% significance level. 29

Fig. 3. NCEP ENSO DJF composite anomalies of (a) zonal wind at 200mb (u'_{200}, contour interval is 2 m s^{-1}), (b) u'_{200} baroclinic component (contour interval is 2 m s^{-1}), (c) zonal wind at 1000mb (u'_{1000}, contour interval is 1 m s^{-1}), and (d) u'_{1000} baroclinic component (contour interval is 1 m s^{-1}). Shading denotes regions where the anomaly passes a two-sided t-test at the 95% significance level. 30

Fig. 4. NCEP ENSO DJF composite anomaly of barotropic component of zonal wind ($u_0{}'$, contour interval is 1 m s^{-1}). Shading denotes regions where the anomaly passes a two-sided t-test at the 95% significance level. 31

Fig. 5. NCEP ENSO DJF composite anomalies of (a) the barotropic RWS, (b) shear advection contribution, (c) vertical advection contribution, (d) surface drag contribution, (e) the residual, and (f) the barotropic RWS plus the residual (total). The box indicates the Pacific region where the forcing is applied in the QTCM experiments, values outside the region is set to zero. The units are (x10^{-11} s^{-2}). Stippling denotes regions where the anomaly passes a two-sided t-test at the 95% significance level. 32

Fig. 6. QTCM DJF barotropic wind anomalies ($u_0{}'$) forced with (a) the barotropic RWS forcing, (b) shear advection forcing, (c) vertical advection forcing, (d) surface drag forcing, (e) the residual forcing, and (f) total forcing (the barotropic RWS plus the residual forcing) in Fig. 5. The units are m s^{-1}. Shading denotes regions where the anomaly passes a two-sided t-test at the 95% significance level. 33

Fig. 7. Shear advection term decomposition: (a) the largest term in the shear advection Rossby wave source anomaly, RWS$'_{shear}$: $\frac{\partial}{\partial y}\left\langle \bar{u}_1 \frac{\partial u_1{}'}{\partial x} + \bar{v}_1 \frac{\partial u_1{}'}{\partial y} \right\rangle$, (b) the largest term in shear advection contribution without curl: $\left\langle \bar{u}_1 \frac{\partial u_1{}'}{\partial x} + \bar{v}_1 \frac{\partial u_1{}'}{\partial y} \right\rangle$, (c) the u component: $\left\langle \bar{u}_1 \frac{\partial u_1{}'}{\partial x} \right\rangle$, and (d) the v component: $\left\langle \bar{v}_1 \frac{\partial u_1{}'}{\partial y} \right\rangle$. Black ovals in panel c highlight regions of strong $\left\langle \bar{u}_1 \frac{\partial u_1{}'}{\partial x} \right\rangle$ shear advection discussed in the text. 34

Fig. 8. Schematic based on the ENSO temperature and wind anomalies of Fig. 2, and the regions of large shear interaction in Fig. 7, indicating relationships between the ENSO baroclinic wind anomalies and the baroclinic climatological shear. Black ovals correspond to those in Fig. 7c, highlighting regions of strong $\left\langle \bar{u}_1 \frac{\partial u_1{}'}{\partial x} \right\rangle$ shear advection. 35

Fig. 9. Vertical advection term decomposition: (a) the largest term in vertical advection: $\frac{\partial}{\partial y}\left\langle (\frac{\partial u_1{}'}{\partial x} + \frac{\partial v_1{}'}{\partial y})\bar{u}_1 \right\rangle$, (b) the largest term in vertical advection without curl: $\left\langle (\frac{\partial u_1{}'}{\partial x} + \frac{\partial v_1{}'}{\partial y})\bar{u}_1 \right\rangle$, and (c) vertical average of vertical velocity anomaly: $\langle \omega' \rangle$. 36

Fig. A1. Same as in Fig. 6 in the main text except for QTCM DJF 200mb baroclinic wind anomalies ($u_{200}{}'$-baroclinic; units m s^{-1}). These are associated with the barotropic solution forced by the barotropic RWS in the barotropic equation. Shading denotes regions where the anomaly passes a two-sided t-test at the 95% significance level. 37

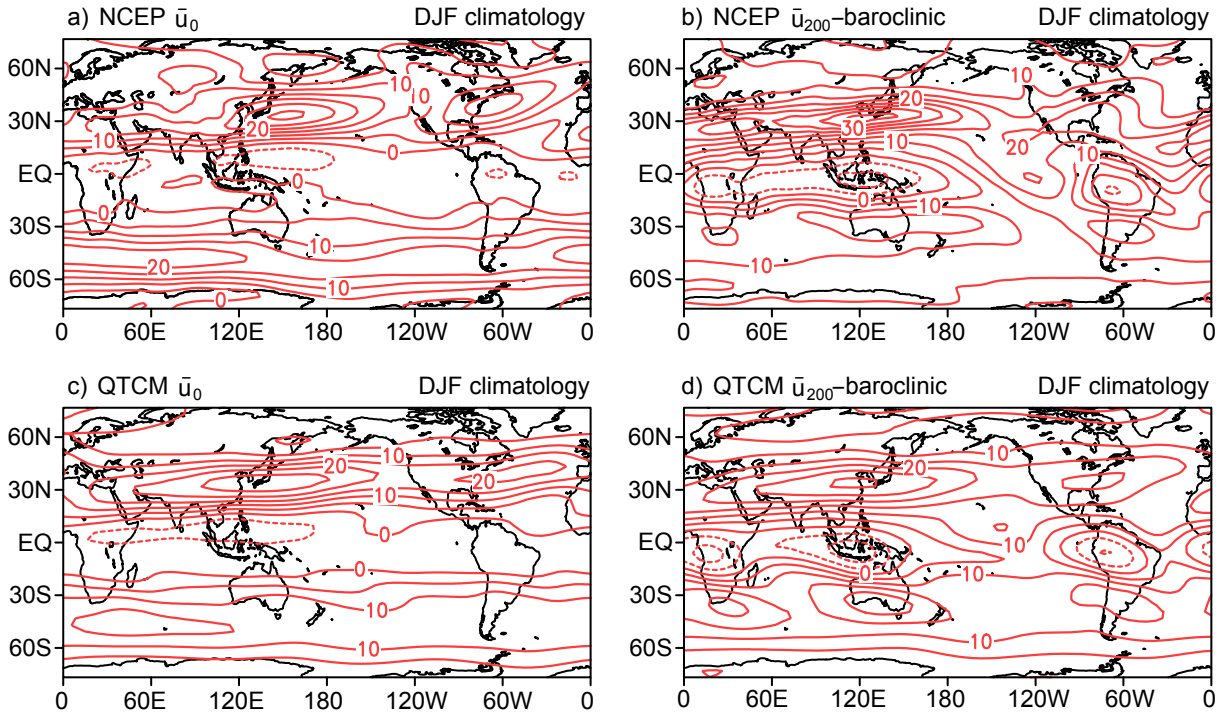

FIG. 1. DJF climatology of (a) NCEP barotropic zonal wind ($\bar{u}_0$), (b) NCEP baroclinic zonal wind at 200mb ($\bar{u}_{200}$-baroclinic), (c) $\bar{u}_0$ from a 100yr QTCM run with climatological SSTs, and (d) QTCM $\bar{u}_{200}$-baroclinic. The units are m s $^{-1}$.

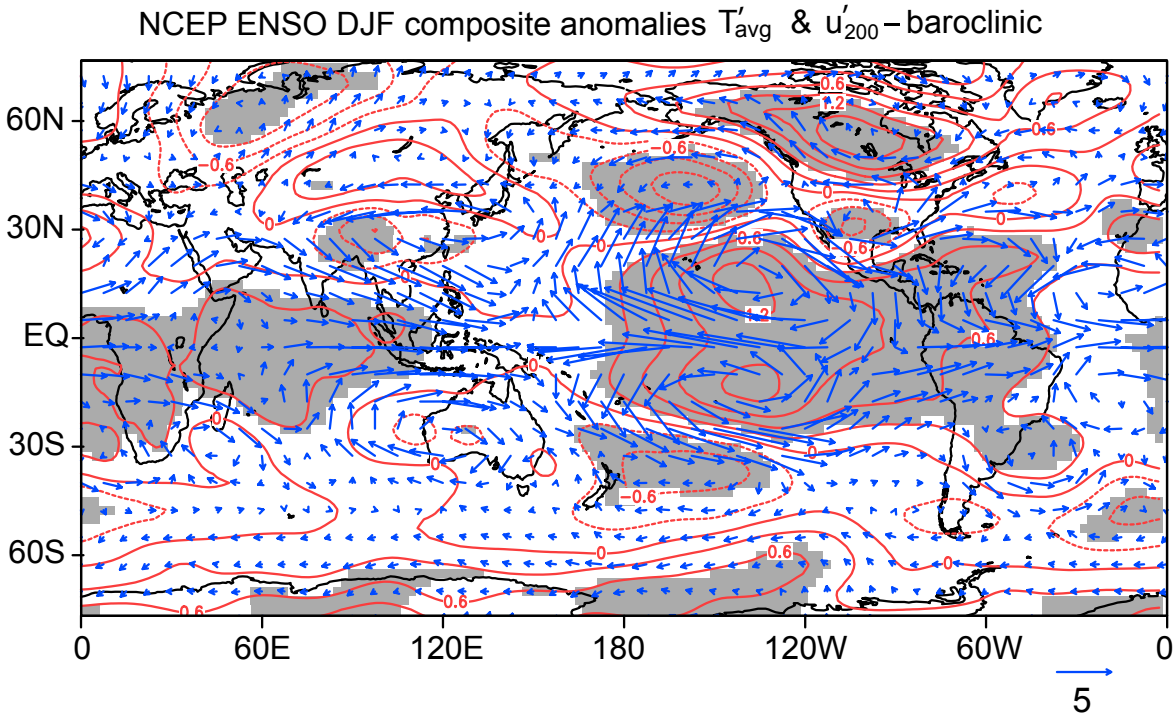

FIG. 2. NCEP ENSO DJF composite anomalies of vertically averaged tropospheric temperature (T'_{avg}) and 200mb baroclinic wind (u'_{200}-baroclinic). The units are K for temperature, and m s^{-1} for winds. Shading denotes regions where the temperature anomaly passes a two-sided t-test at the 95% significance level.

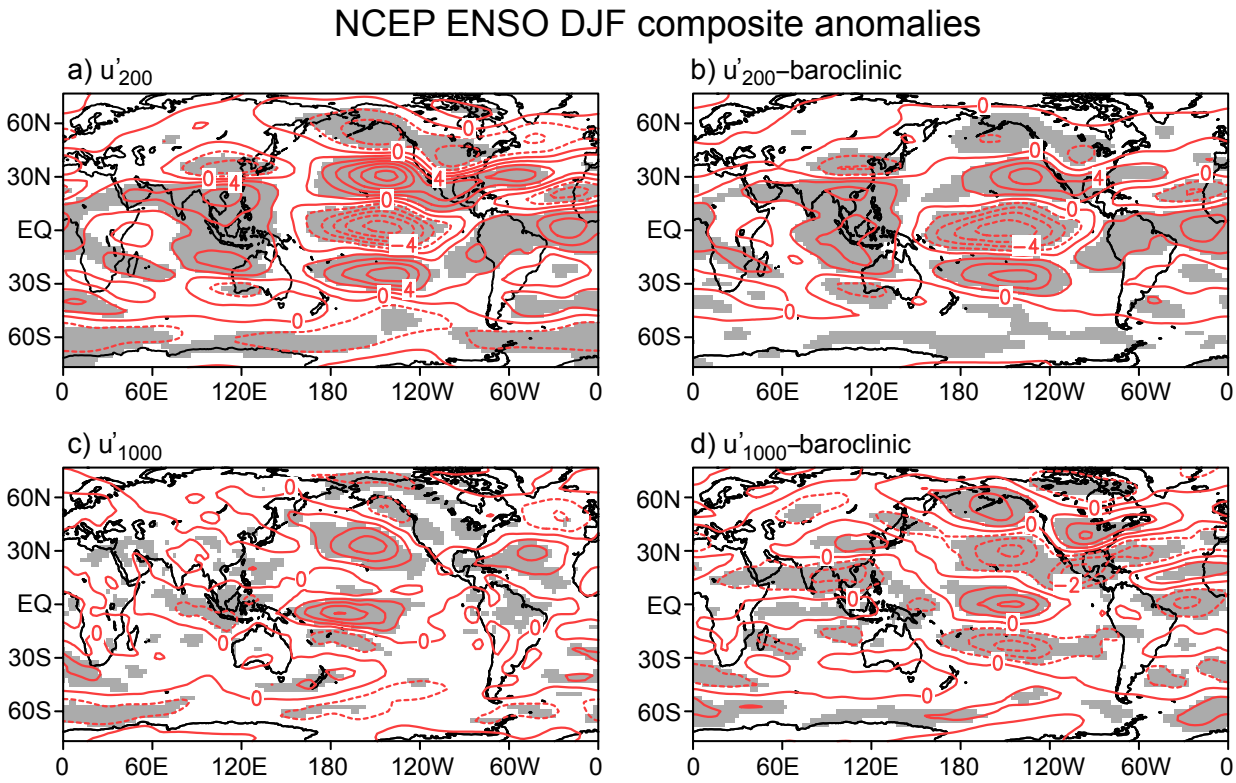

FIG. 3. NCEP ENSO DJF composite anomalies of (a) zonal wind at 200mb (u'_{200}, contour interval is 2 m s^{-1}), (b) u'_{200} baroclinic component (contour interval is 2 m s^{-1}), (c) zonal wind at 1000mb (u'_{1000}, contour interval is 1 m s^{-1}), and (d) u'_{1000} baroclinic component (contour interval is 1 m s^{-1}). Shading denotes regions where the anomaly passes a two-sided t-test at the 95% significance level.

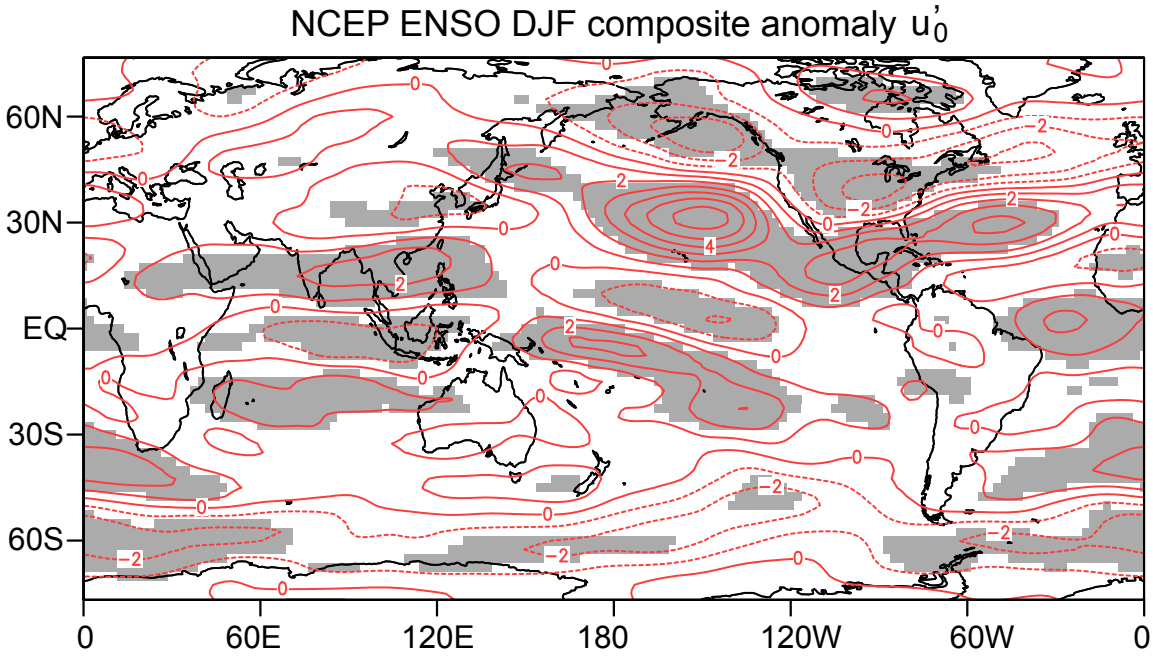

FIG. 4. NCEP ENSO DJF composite anomaly of barotropic component of zonal wind ($u_0{}'$, contour interval is 1 m s^{-1}). Shading denotes regions where the anomaly passes a two-sided t-test at the 95% significance level.

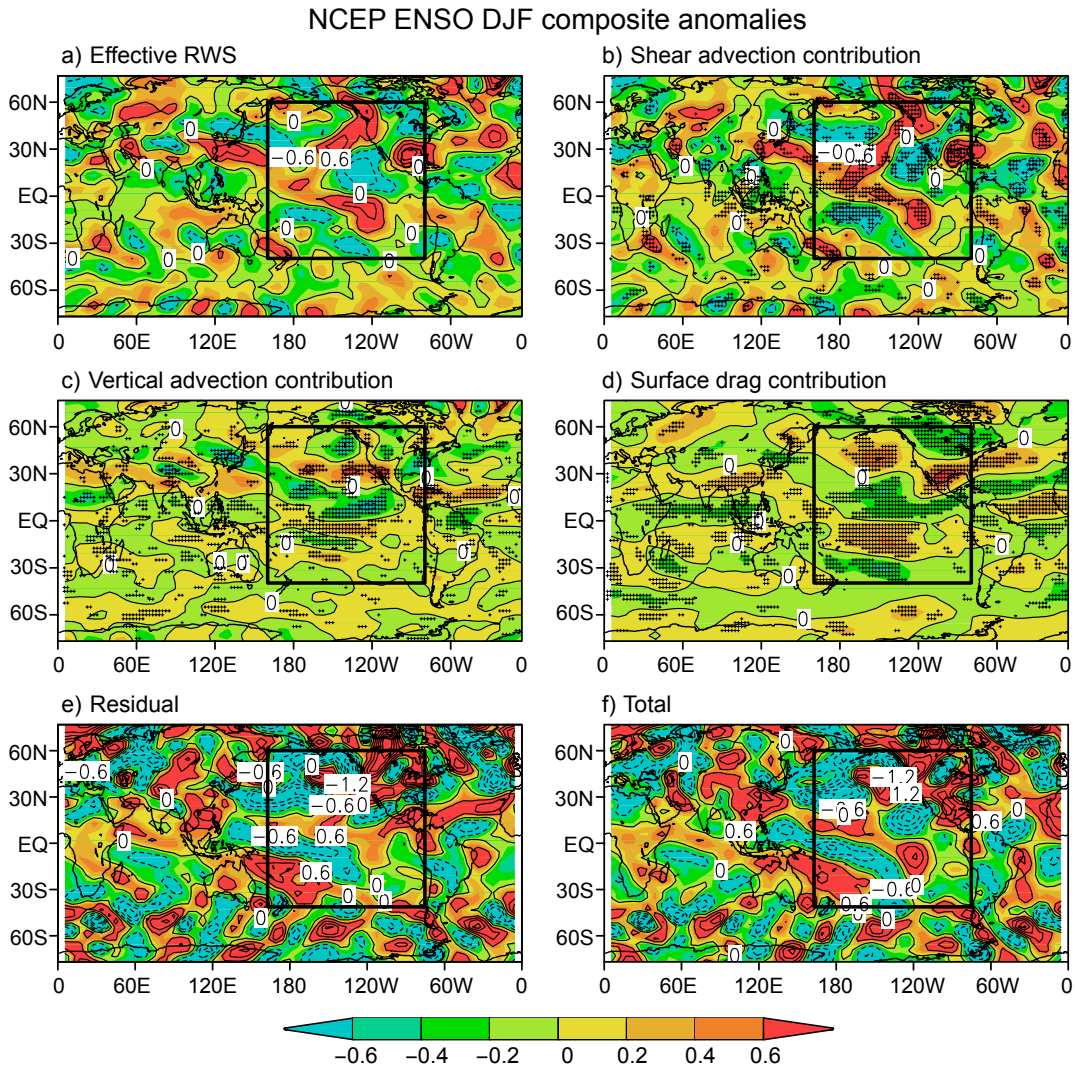

FIG. 5. NCEP ENSO DJF composite anomalies of (a) the barotropic RWS, (b) shear advection contribution, (c) vertical advection contribution, (d) surface drag contribution, (e) the residual, and (f) the barotropic RWS plus the residual (total). The box indicates the Pacific region where the forcing is applied in the QTCM experiments, values outside the region is set to zero. The units are (x10^{-11} s^{-2}). Stippling denotes regions where the anomaly passes a two-sided t-test at the 95% significance level.

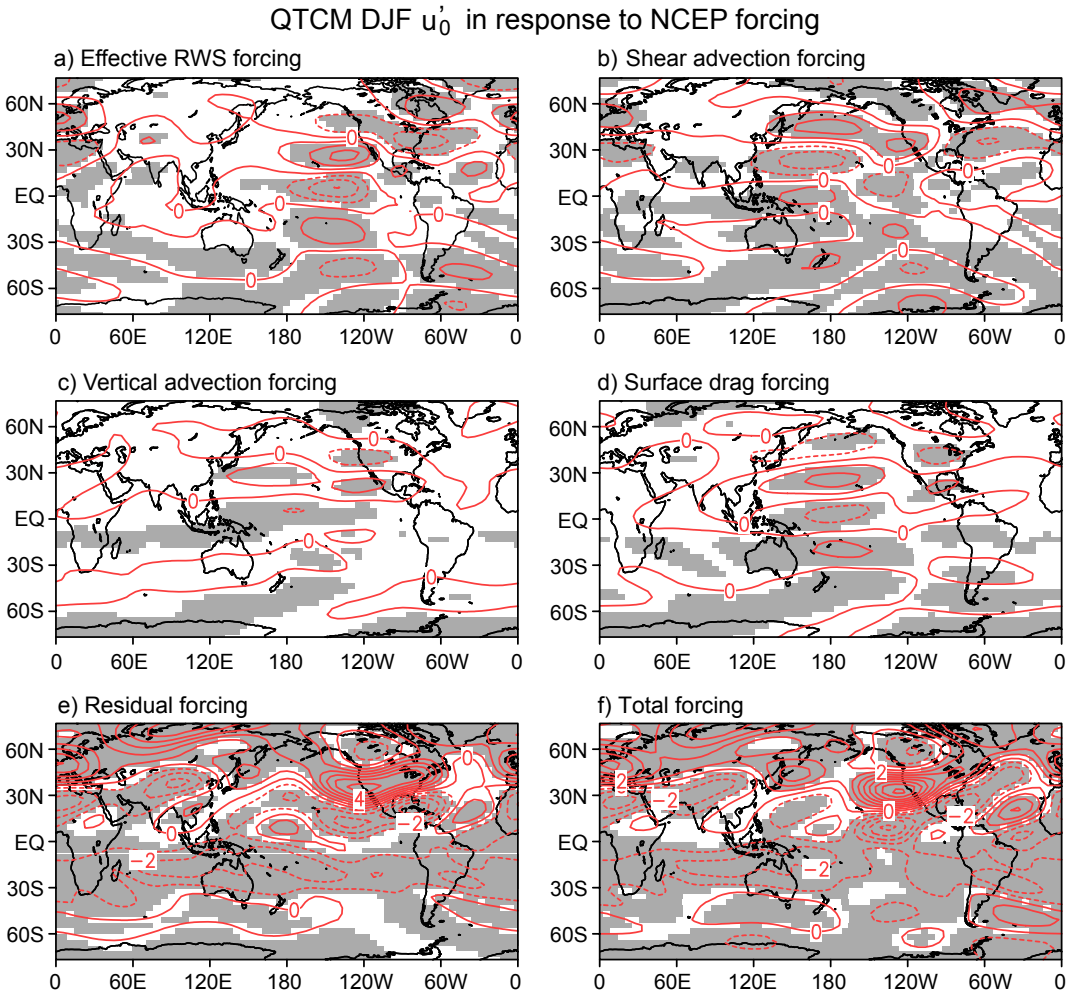

FIG. 6. QTCM DJF barotropic wind anomalies ($u_0{}'$) forced with (a) the barotropic RWS forcing, (b) shear advection forcing, (c) vertical advection forcing, (d) surface drag forcing, (e) the residual forcing, and (f) total forcing (the barotropic RWS plus the residual forcing) in Fig. 5. The units are m s^{-1}. Shading denotes regions where the anomaly passes a two-sided t-test at the 95% significance level.

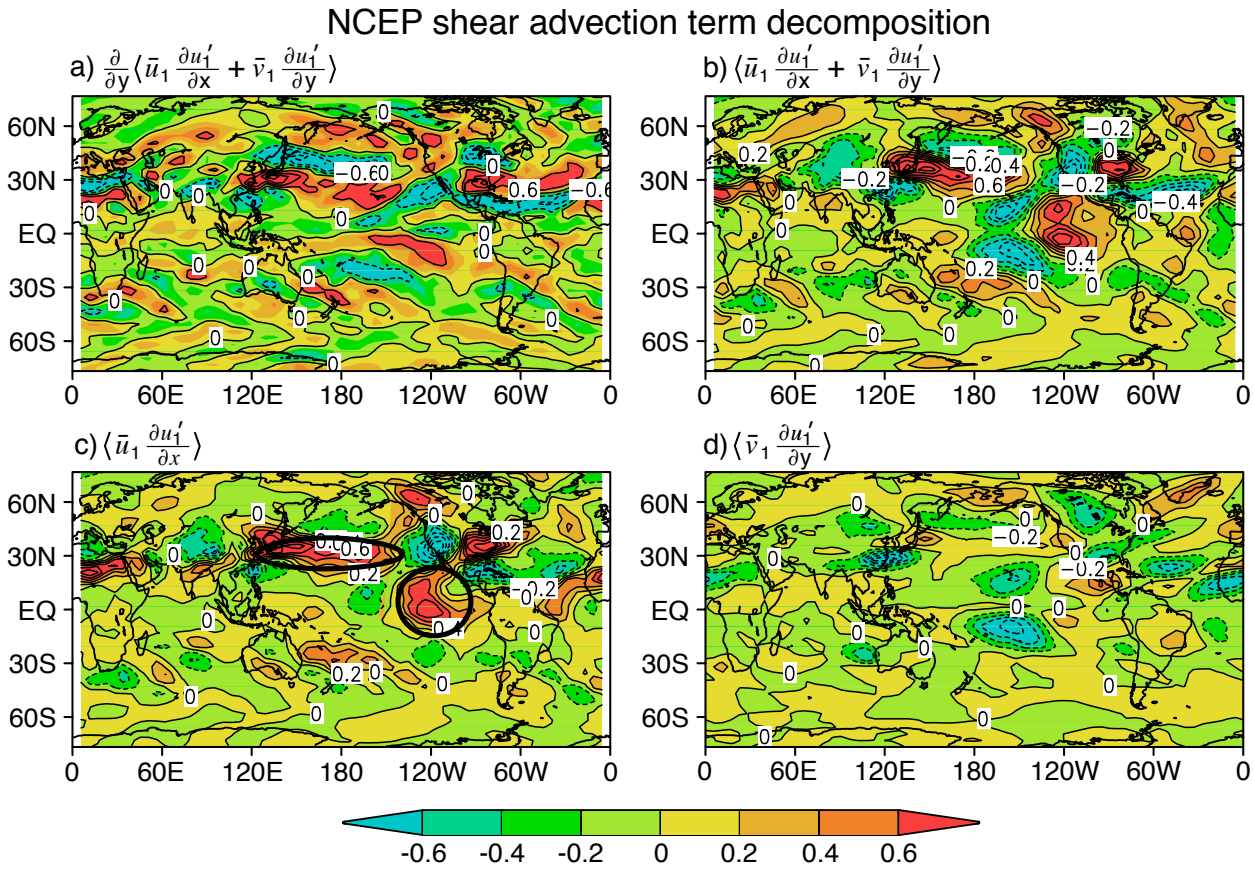

FIG. 7. Shear advection term decomposition: (a) the largest term in the shear advection Rossby wave source anomaly, RWS'_{shear}: $\frac{\partial}{\partial y}\left\langle \bar{u}_1 \frac{\partial u_1{}'}{\partial x} + \bar{v}_1 \frac{\partial u_1{}'}{\partial y} \right\rangle$, (b) the largest term in shear advection contribution without curl: $\left\langle \bar{u}_1 \frac{\partial u_1{}'}{\partial x} + \bar{v}_1 \frac{\partial u_1{}'}{\partial y} \right\rangle$, (c) the u component: $\left\langle \bar{u}_1 \frac{\partial u_1{}'}{\partial x} \right\rangle$, and (d) the v component: $\left\langle \bar{v}_1 \frac{\partial u_1{}'}{\partial y} \right\rangle$. Black ovals in panel c highlight regions of strong $\left\langle \bar{u}_1 \frac{\partial u_1{}'}{\partial x} \right\rangle$ shear advection discussed in the text.

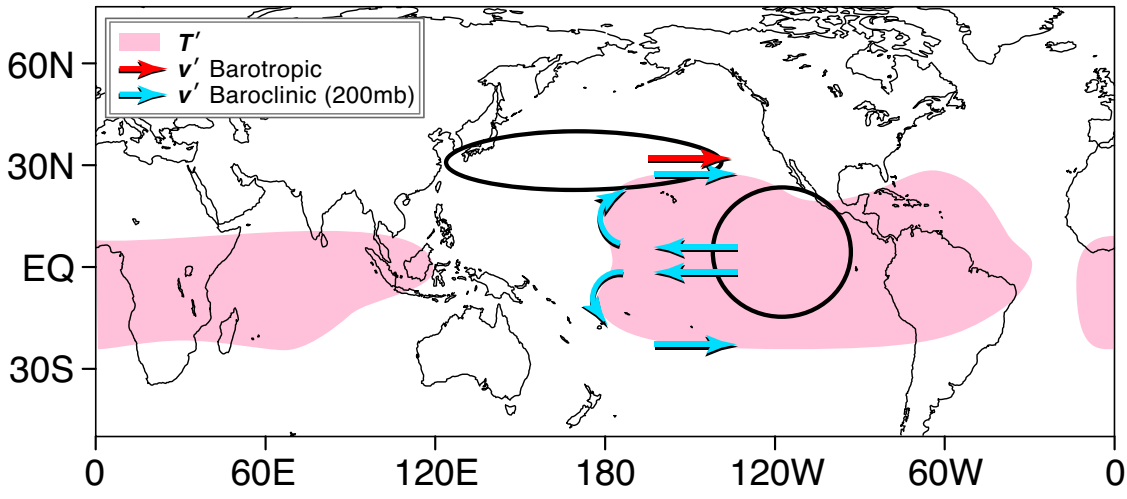

FIG. 8. Schematic based on the ENSO temperature and wind anomalies of Fig. 2, and the regions of large shear interaction in Fig. 7, indicating relationships between the ENSO baroclinic wind anomalies and the baroclinic climatological shear. Black ovals correspond to those in Fig. 7c, highlighting regions of strong $\left\langle \bar{u}_1 \frac{\partial u_1{}'}{\partial x} \right\rangle$ shear advection.

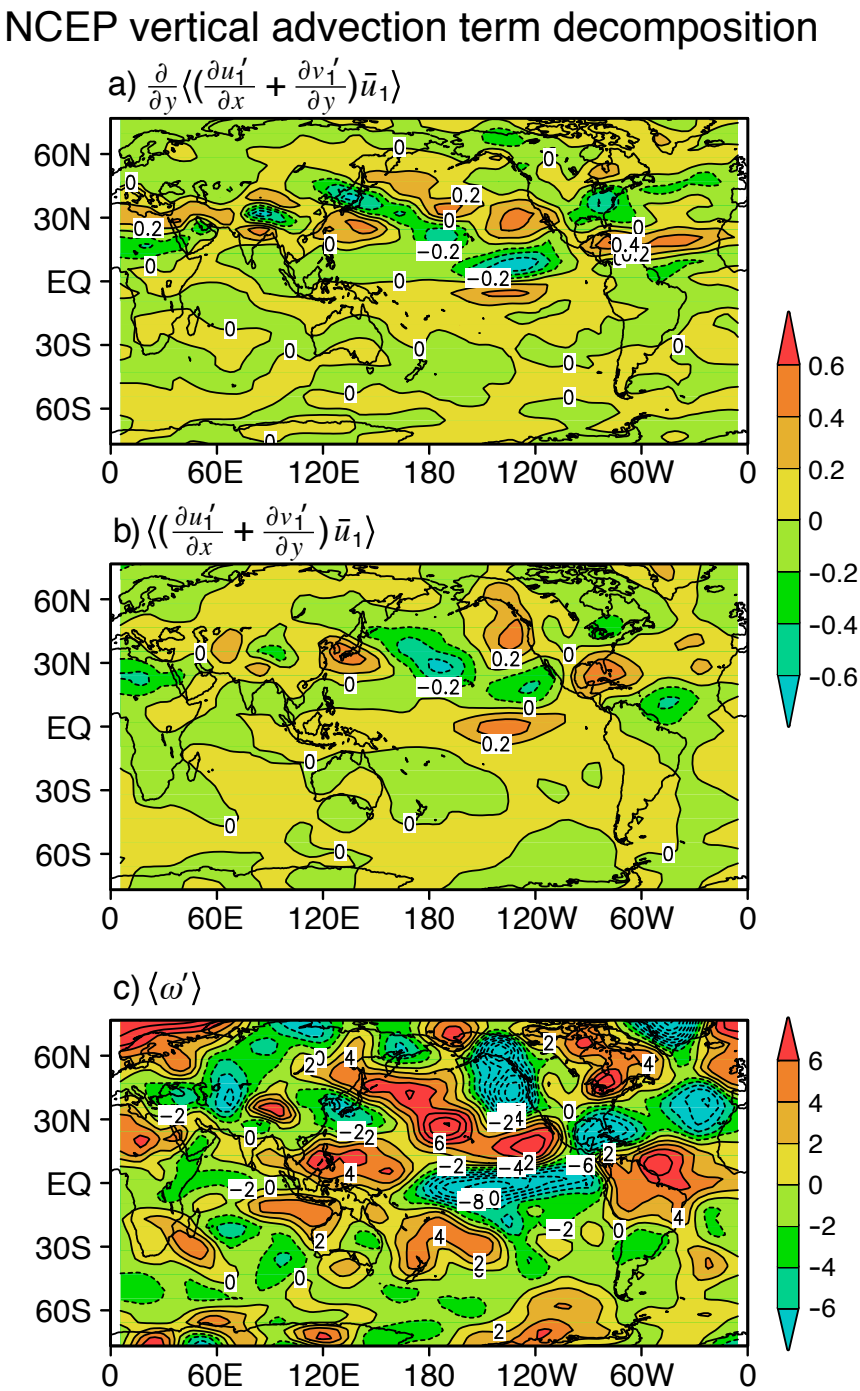

FIG. 9. Vertical advection term decomposition: (a) the largest term in vertical advection: $\frac{\partial}{\partial y}\left\langle(\frac{\partial u_1{}'}{\partial x}+\frac{\partial v_1{}'}{\partial y})\bar{u}_1\right\rangle$, (b) the largest term in vertical advection without curl: $\left\langle(\frac{\partial u_1{}'}{\partial x}+\frac{\partial v_1{}'}{\partial y})\bar{u}_1\right\rangle$, and (c) vertical average of vertical velocity anomaly: $\langle\omega'\rangle$.

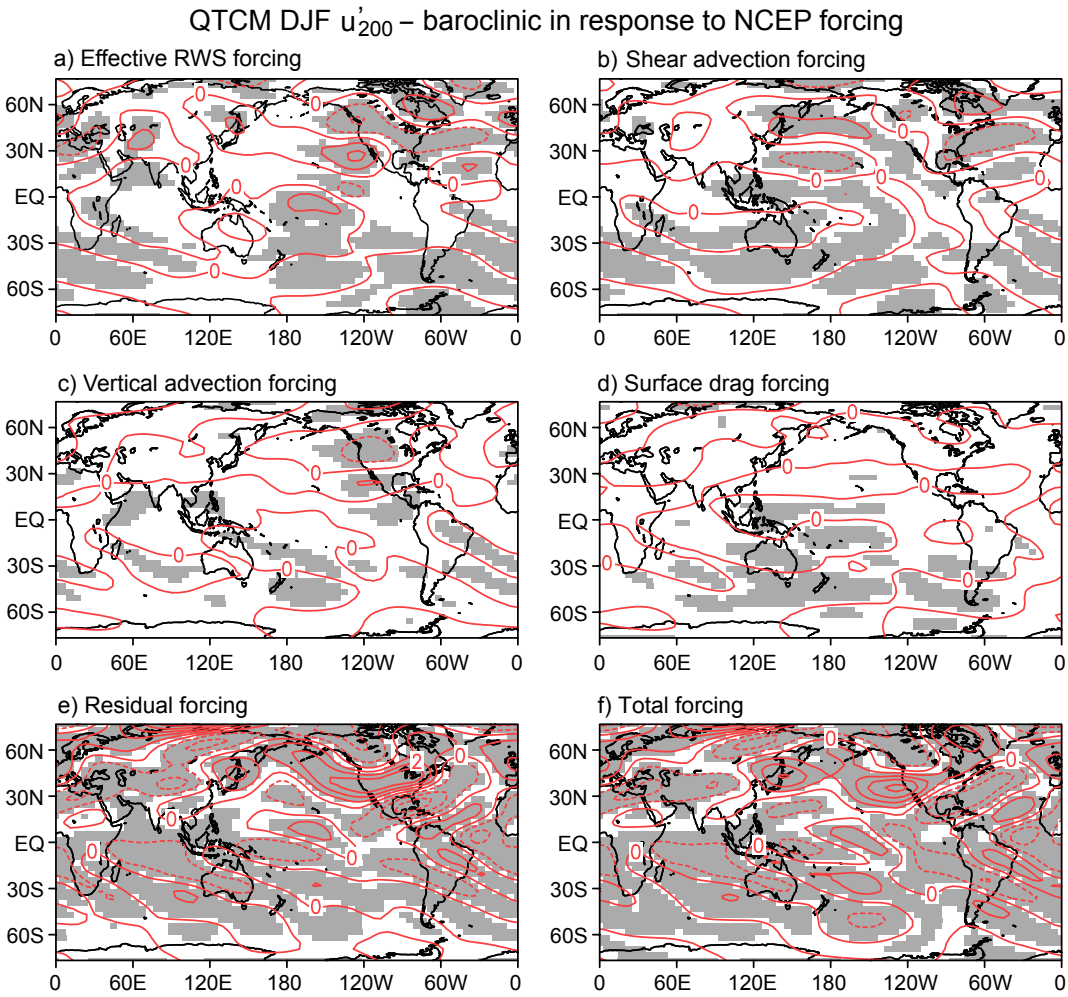

Fig. A1. Same as in Fig. 6 in the main text except for QTCM DJF 200mb baroclinic wind anomalies ($u_{200}{}'$-baroclinic; units m s^{-1}). These are associated with the barotropic solution forced by the barotropic RWS in the barotropic equation. Shading denotes regions where the anomaly passes a two-sided t-test at the 95% significance level.